Characterization of pixel sensor prototypes for the Muon Forward Tracker at ALICE

Graduate School of Science, Hiroshima University
Department of Physical Science

Experimental Quark Physics Laboratory

Akihide Nobuhiro
M153475

Supervisor	:	Associate Prof. Kenta Shigaki
Primary examiner	:	Associate Prof. Kenta Shigaki
Examiner	:	Associate Prof. Makoto Uemura

10th.February.2017

Abstract

We plan to install MFT (Muon Forward Tracker) at ALICE (A Large Ion Collider Experiment) for the LHC Run 3 from 2021. It will allow us muon and di muon measurements in the lower transverse momentum region with a higher resolution. A new pixel sensor, called ALPIDE (ALICE pixel detector) which is based on the MAPS (Monolithic Active Pixel Sensor) technology, which satisfies stringent requirements such as the high detection efficiency, the fast integration time, and low fake hit rate will be used for MFT. The sensor will be fabricated using the 180 nm CMOS imaging sensor process by TowerJazz. A particular advantage of this technology is that it is possible to collect full charges which are ionized at the epitaxial layer. In addition, ALPIDE provides the possibility to apply the reverse bias to the collection electrode in order to adjust the depletion region.

I built the test system for prototypes of ALPIDE (pALPIDE) and characterized them for the first time in Japan. The final ALPIDE design is decided from prototypes by the ITS group which started the study earlier than the MFT group, but ALPIDE and pALPIDE still need to be tested to optimize the settings and it is necessary to accumulate the experience in order to operate ALPIDE for the MFT institutes. The threshold and the noise or fake hit rate and efficiency can be adjusted by controlling current and voltage values, called V_{CASN} and I_{THR} in the front end circuit for shaping corrugations, when the charges generated by ionizing incident particles are detected as the signal. In this study, I characterized the pALPIDE versions 2 and 3. It was confirmed that the threshold value increases as V_{CASN} increases, and it decreases as I_{THR} decreases. It was also confirmed that the noise occupancy increases when the temperature of the sensor increases, and the fake hit rate and relative efficiency decreases by increasing I_{THR}. These results obtained by the characterization are very important data for us to operate MFT in the near future

Contents

1 Introduction **6**
- 1.1 Quark Gluon Plasma(QGP) . . . 6
- 1.2 High energy heavy ion collisions . . . 6
- 1.3 ALICE (A Large Ion Collider Experiment) . . . 7
- 1.4 Muon measurements . . . 7
- 1.5 Motivation of this thesis . . . 9

2 MFT in ALICE upgrade plans **10**
- 2.1 ALICE upgrade plan . . . 10
- 2.2 Muon Spectrometer . . . 10
- 2.3 Positioning resolution . . . 11
- 2.4 MFT . . . 11

3 MAPS technology and ALPIDE development for MFT **13**
- 3.1 Required pixel sensor performance . . . 13
- 3.2 MAPS technology . . . 13
- 3.3 ALPIDE design . . . 13
- 3.4 Matrix isolation of ALPIDE chip . . . 14
- 3.5 Charge generation in the epitaxial layer . . . 15
- 3.6 Reverse substrate bias and depletion region . . . 15
- 3.7 Roadmap of ALPIDE development . . . 16

4 ALPIDE and pALPIDE structure **18**
- 4.1 ALPIDE and pALPIDE rough structure . . . 18
- 4.2 Detail of the front end circuit of pALPIDE . . . 19
  - 4.2.1 pALPIDE-2 . . . 19
  - 4.2.2 pALPIDE-3 . . . 20
  - 4.2.3 Front end biasing parameters . . . 21
- 4.3 Digital part of pALPIDE . . . 21
- 4.4 Front end circuit of ALPIDE . . . 23

5 pALPIDE version 2 and 3 characterization **24**
- 5.1 Construction of the experimental environment for pALPIDE . . . 24
- 5.2 Threshold scan . . . 25
- 5.3 Threshold and noise . . . 25
- 5.4 Fake hit rate . . . 27
- 5.5 Temperature dependence . . . 30
- 5.6 Source measurement . . . 30
- 5.7 Relative efficiency . . . 33

6 Summary and Outlook **35**

Acknowledgment **36**

Reference **37**

List of Figures

1 A schematic diagram of atomic structure. 6
2 A schematic diagram of space time evolution of a heavy ion collision[1]. 7
3 ALICE detectors[1]. 8
4 Transverse momentum and momentum. 8
5 Structure of Muon Spectrometer 11
6 Particle reconstruction without MFT (top) and with MFT (bottom). The red line shows the real track and the blue line shoes the incorrect track. 12
7 Structure of MFT 12
8 A schematic cross section of a pixel sensor with MAPS technology . 14
9 A pixel chip architecture of ALPIDE 14
10 A schematic of matrix isolation in the ALPIDE design. 15
11 Schematics cross section of ALPIDE design 16
12 The depletion region of ALPIDE with low (top) and high (bottom) reverse substrate bias. 16
13 The roadmap of ALPIDE development and features. 17
14 The real pALPIDE-2 chip. 18
15 The pixel layout and pixel matrix details of a pALPIDE-2[10]. . . . 18
16 The schematic of a pixel circuit of pALPIDE and its signal flow. . . 19
17 A front end circuit diagram of a pALPIDE-2 including all possible variations[11]. 19
18 A schematic of the diode reset (left) and PMOS reset (right). 20
19 The front end circuit of pALPIDE-3 including all possible variations[11]. 20
20 The schematic of the input transistor M1. Connect V_{DDA} (right) or connect V_{SOURCE} (left) to the body terminal. 21
21 A schematic of a section of the state register in a pALPIDE[12]. . . 23
22 A schematic of the front end circuit in pALPIDE[11]. 23
23 The carrier board (left) and DAQ board (right). 24
24 The wiring diagram of the equipment. 24
25 The test environment at Hiroshima University. 25
26 The number of hit charges as the function of the injected charges. . 26
27 Threshold values and their numbers in each sector for pALPIDE-2 with $I_{THR} = 10$ (upper left), $I_{THR} = 50$ (upper right) and $I_{THR} = 100$ (bottom left). 26
28 Threshold values and their numbers in each sector for pALPIDE-2 with $I_{THR} = 50$ / $V_{BB} = -3\,V$ / $V_{RST} = 117$ (upper left) and $V_{RST} = 140$ (upper right), and $I_{THR} = 50$ / $V_{BB} = -6\,V$ / $V_{RST} = 117$ (bottom left) and $V_{RST} = 180$ (bottom right). 27
29 Threshold values vs I_{THR} in each sector for pALPIDE-2 with $V_{BB} = -0\,V$ (upper left) ,-3 V (upper right) and -6 V (bottom left). 28
30 Noise values vs I_{THR} in each sector for pALPIDE-2 with $V_{BB} = -0\,V$ (upper left) ,-3 V (upper right) and -6 V (bottom left). 28
31 Threshold (left) and noise (right) values and their number in each sector for pALPIDE-3 with $V_{BB} = -0\,V$ / $I_{THR} = 50$. 29
32 The threshold values vs I_{THR} in each sector for pALPIDE-3 with $V_{BB} = -0\,V$ (upper left) ,-3 V (upper right) and -6 V (bottom left). 29

33 The noise values vs I_{THR} in each sector for pALPIDE-3 with $V_{BB} = -0\,V$ (upper left) ,-3 V (upper right) and -6 V (bottom left). 30
34 I_{THR} dependence of fake hit rate in each sector for pALPIDE-3 with $V_{BB} = -0\,V$ (upper left) ,-3 V (upper right) and -6 V (bottom left). 31
35 V_{CASN} dependence of fake hit rate in each sector for pALPIDE-3 with $V_{BB} = -0\,V$ (upper left) ,-3 V (upper right) and -6 V (bottom left). 31
36 Temperature of pALPIDE over time and number of hits without a source at that time. 32
37 Source (Fe55) used in the experiment. 32
38 Hit map without source (left) and with source (right) for pALPIDE-3. 32
39 Clustering method. 33
40 Hit map (left) and cluster (right) map for pALPIDE-3 with source. . 33
41 Cluster size distribution for pALPIDE-3 with source (left, red line) and without source (left, blue line), and its difference (right). 33
42 I_{THR} dependence of cluster size. 34
43 I_{THR} dependence of relative efficiency and the fake hit rate. 34

1 Introduction

The basic acknowledge and the background of this study are described in this section.

1.1 Quark Gluon Plasma(QGP)

All substances such as our body and the star such as the earth and the sun are collective objects of atoms. An atom is composed of leptons such as electrons . The nuclei is composed of proton and neurons, and protons and neutrons are composed of quarks considered to be the smallest particle as shown in Fig1. Quarks are bound by a strong interaction, which is propagated by gluons. According to QCD (Quantum Chromo-Dynamics) which describes this law of physics, quarks have the property that they can not be removed alone normally from a nucleon. However, this law is broken in high temperature, high density, and in the plasma state, called QGP (Quark Gluon Plasma). QGP is present when the quark and the gluon exist in a separated state. It is thought that QGP was present inside the neutron star or in the very early universe between 10^{-6} and 10^{-5} seconds where the high temperature and high density state is maintained. Elucidation of the physical properties related to QGP is a very important study leading to elucidation of physics such as the formation of the universe and the generation of various particles, but it is impossible to see the state which existed more than 10 billion years ago or the star which is far from tens of thousands light years directly. However, it is possible to generate QGP which is a high temperature and high density state in a very limited time and space by colliding heavy nuclei with high energy.

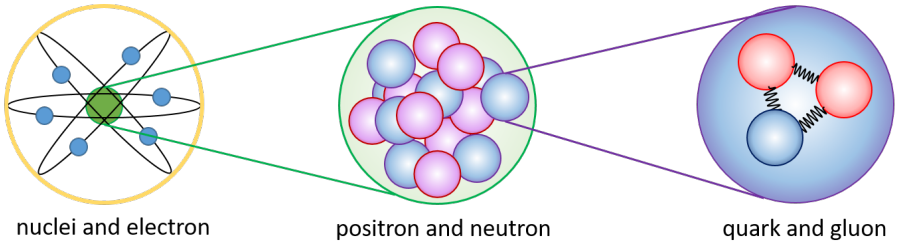

Figure 1: A schematic diagram of atomic structure.

1.2 High energy heavy ion collisions

The quarks and gluons break the confinement shell and QGP is generated when heavy ions collide at a speed of 99.9999% or faster than the speed of light with an accelerator. These properties are studied by detecting the particles generated in each process from the start to the end of collisions. Heavy ion collisions follow space time development as shown in Fig.2. Heavy ions accelerated by the accelerator appear as flat disks like a pancake due to Lorentz contraction. Immediately after the collision, the temperature and the energy density of the participant increases. Then the parton, which is the generic name of a quark and gluon, is released from the confinement of the hadron. They scatter freely and collide with each other, and generate a new parton. This state is called QGP. QGP expands rapidly, the temperature and the density decrease, and some partons generate hadrons by recombination. Furthermore, the temperature and the density of the system decreases, inelastic scatterings

of the hadrons disappear, and the interactions between the quarks also disappear. A scientifically frozen state in which no new particles are generated is obtained. The expansion continues, elastic collisions between the hadrons also disappear, and particles obtain a fixed momentum. Generated particles reach the detector while maintaining the information and are observed. These are being studied every day using LHC (Large Heavy ion Collider) at CERN (European Organization for Nuclear Research) etc.

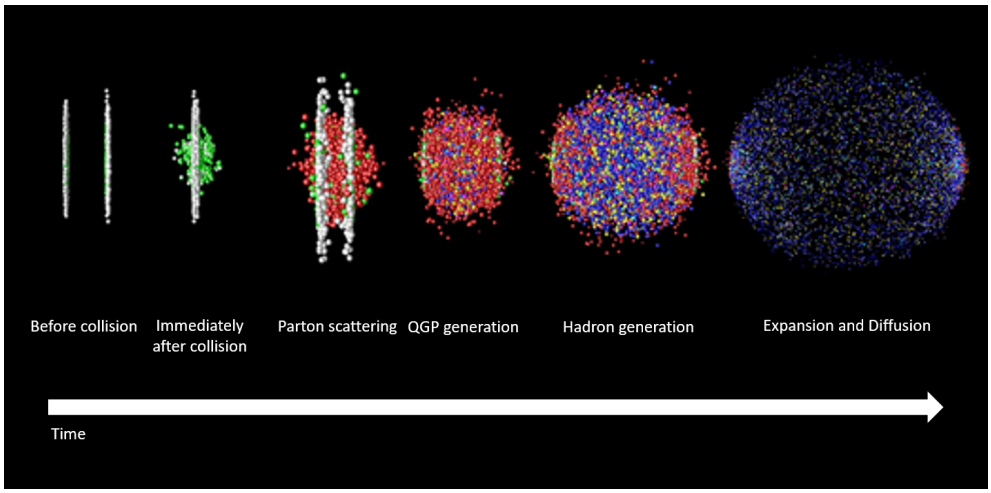

Figure 2: A schematic diagram of space time evolution of a heavy ion collision[1].

1.3 ALICE (A Large Ion Collider Experiment)

Various aspects of physics are studied by six groups (ATLAS and CMS which discovered higgs, LHCb, LHCf, TOTEM and ALICE) in the high energy particle collisions experiment using LHC. ALICE, which Hiroshima University belongs, is an experimental group specialized for heavy ion collisions and the large scale international collaborative experiment. In order to detect various particles such as electrons and muons which are leptons and quarks such as charm and strange generated by heavy ion collisions, multiple detectors are incorporated around the collision points at ALICE as shown in Fig3. ALICE detectors are roughly divided into central barrels such as ITS and PHOS that handle the near collision points. The Muon Arm that handles muons in the forward direction, and global detectors that select events such as V0 detectors. It is expected to elucidate the properties of QGP, the state of the very early universe, the properties of substances at high temperature and density, etc.

1.4 Muon measurements

In order to study QGP, particles generated and passed over time in QGP should be watched in a wide range of transverse momentum shown in Fig.4. Many measurements are performed using electrons and hadrons as probes for analysis, but in the low transverse momentum region, highly accurate analysis is difficult to obtain because there is a lot of background interactions which makes it difficult to see. Recently, measurements using muon which is lepton as a probe for analysis are

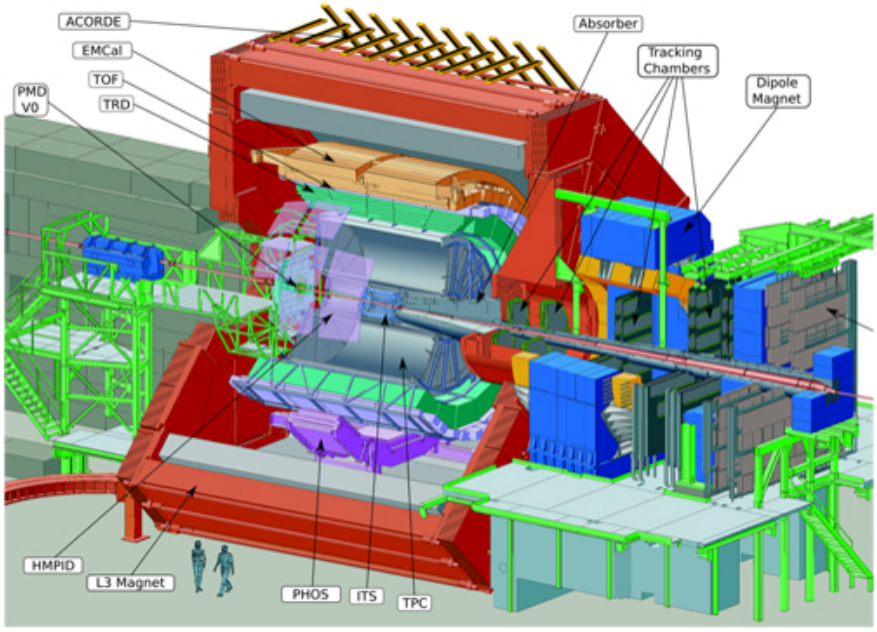

Figure 3: ALICE detectors[1].

drawing attention. Muon have properties that are very suitable for analysis in the low transverse momentum region such as having no strong interaction. They hardly cause bremsstrahlung and have extremely high permeability. Since muons do not have strong interaction, they do not receive unnecessary influence from others when passing through QGP. So muons reach the detector with the information at the time of generation. High permeability allow that only muon is detected by mounted the absorber in front of the detector. However, it is necessary to have enough momentum to pass through the absorber. For the above reasons, measurements using muons as probes in the high momentum and low transverse momentum regions are necessary for elucidating QGP properties, but research and development such as improving the resolution of the detector are required.

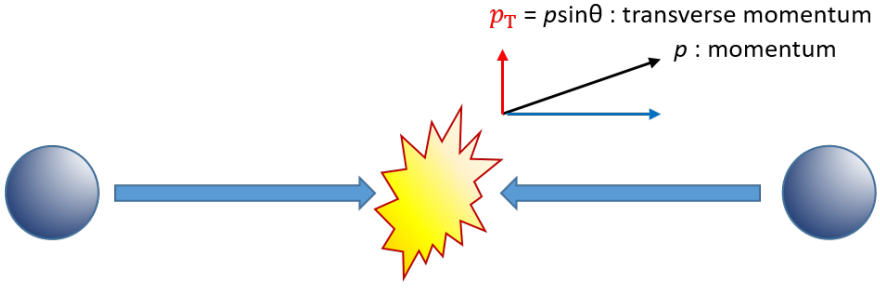

Figure 4: Transverse momentum and momentum.

1.5 Motivation of this thesis

We plan to install MFT (Muon Forward Tracker) at ALICE for the LHC Run3 from 2021. It will allow us muon and di muon measurements in the lower transverse momentum region with a higher resolution. It is expected to explain the very interesting physics leading to QGP understanding such as the measurement of heavy flavor in low transverse momentum regions and chiral symmetry breaking and restoration. I characterize pixel sensor prototypes for the purpose of accumulating experience and data to optimize the sensor of the detector mounted on the MFT in this thesis.

2 MFT in ALICE upgrade plans

The outline of upgrade plans of ALICE and the MFT project I participate are described in this section.

2.1 ALICE upgrade plan

We plan to upgrade ALICE detectors and read out technology. The grate amount of data has been accumulated and analyzed thus far, but studies such as measurements in the low transverse momentum region and of rare events are difficult due to low statistics and resolution. Moreover, it is estimated that the LHC at Run3 will be improved to $6\times10^{27}\,\mathrm{cm}^{-2}\mathrm{s}^{-1}$ for luminosity and 50 kHz in the interaction rate, and it is impossible to read out and accumulate all data for the current one which is the reading speed of 500 Hz for PbPb collisions. Therefore, in order to improve future research, it is planned to upgrade the existing detectors such as an upgraded ITS (Inner Tracking System) and a TPC (Time Projection Chamber), a new detector MFT and a new method of read out technique during the next long shutdown (2019 -2020). The upgrade plan of ALICE is summarized below.

- The ITS will be improved position and transverse momentum resolution, tracking efficiency, and readout rate[2].
- The TPC will be exchanged for a GEM (Gas Electron Multiplier) and new electronics will be mounted. These allow the improvements for enhanced readout performance[3].
- The ZDC (Zero Degree Calorimeter) will be upgraded to accommodate the increased collision rate
- The PHOS (Photon Spectrometer), the TOF (Time of Flight), the TRD (Transition Radiation detector) and the Muon Spectrometer will be upgraded to accommodate the increased readout speed[4].
- The MFT will be added as a new tracker in front of the absorber of muon spectrometer and improve the position resolution[5].
- The O^2 (Online Offline) will be upgraded to allow offline reconstruction and improve continuous readout[6].

2.2 Muon Spectrometer

The Muon Spectrometer is the detector placed in the forward direction of the collision point for muon. As shown in Fig.5, it consists of an absorber, five tracking chambers, an absorber, a trigger chamber and a magnet. It is possible to observe particles that pass through the absorber as muon by using the high permeability of muons. The track of charged particles bent by the magnetic field applied by the magnet is detected by the tracking chamber, and the momentum and mass are reconstructed. Then, the charged particles reaching the trigger chamber are identified as muon.

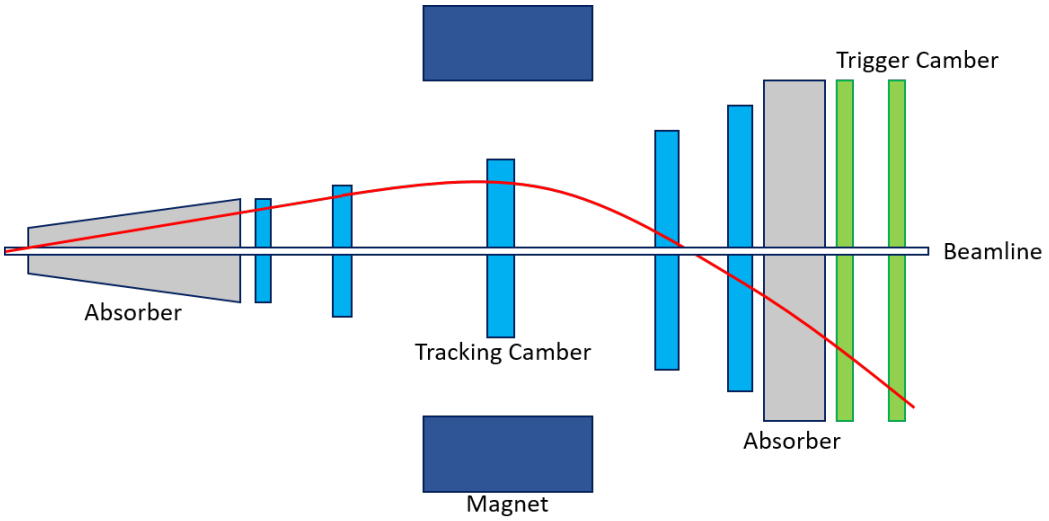

Figure 5: Structure of Muon Spectrometer

2.3 Positioning resolution

Muons are detected by the muon spectrometer, but since there is a distance from the point where the muons are generated to the first tracking chamber and the trajectory of charged particles changes by multiple scattering within the absorber, there is a possibility to not recognize the real track (red line) but recognize the incorrect track (blue line) as the correction shown in Fig6 top. Therefore, a big uncertainty is included in the reconstruction of the generation point. Similarly, since the angle of the muon pair is erroneously measured, resolution of invariant mass identification is low. Now, it is possible to improve the position resolution by mounting a new tracker in front of the absorber as shown in Fig6 bottom. This is MFT.

2.4 MFT

The MFT is located in front of the absorber, in the range of pseudo rapidity of $-3.6<\eta<-2.45$. The size of the detector is about 300 mm in the beam axis direction and detects charged particles with five layer structures. The MFT is made up of two half MFT cones and five disks which are incorporated. The disks have a structure in which ladders with 1 to 5 sensors attached are lined up, and both the front and the back of disks have ladders. Tab.1 shows a summary of the number of each component as shown in Fig.7.

Table 1: Number of each component of MFT[6]

Half disk	0	1	2	3	4	Full
Inner radius (mm)	25.0	25.0	25.0	38.2	39.2	-
Outer radius (mm)	92.6	98.0	104.3	130.1	143.5	-
Number of ladders	24	24	26	32	34	280
Number of sensors	64	64	76	112	132	896

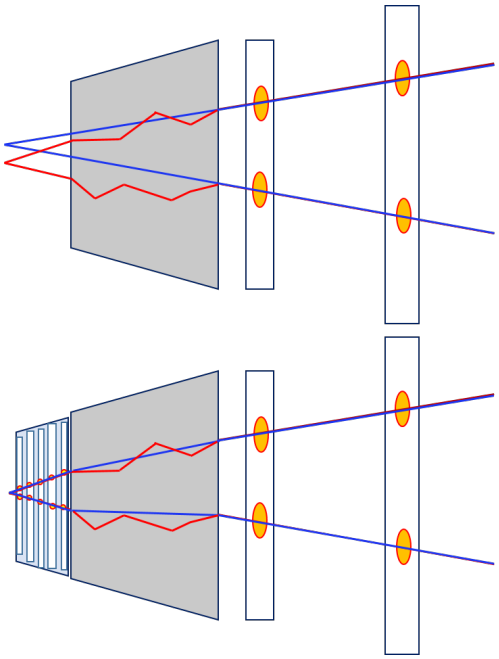

Figure 6: Particle reconstruction without MFT (top) and with MFT (bottom). The red line shows the real track and the blue line shoes the incorrect track.

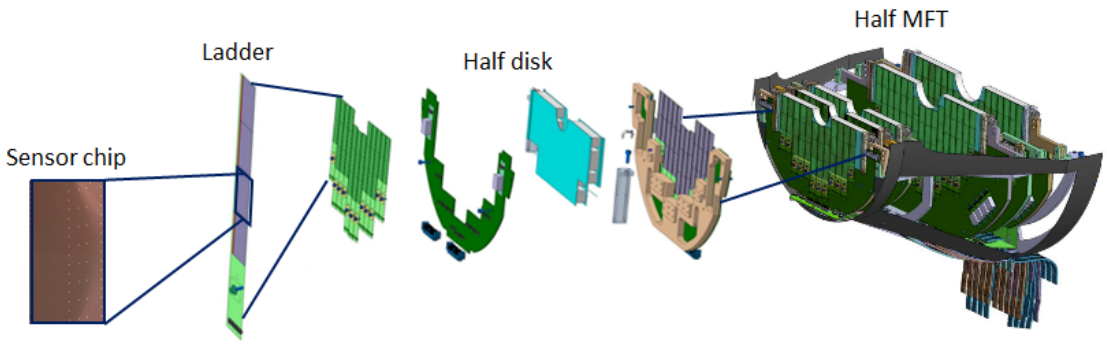

Figure 7: Structure of MFT

3 MAPS technology and ALPIDE development for MFT

Developments of the monolithic silicon pixel chip for the MFT and the improved ITS is called ALPIDE(ALICE pixel detector). ALPIDE which will be fabricated in the 180 nm CMOS sensor process by TowerJazz will be described in this section.

3.1 Required pixel sensor performance

It is important to detect many particles generated by nucleus collisions with high detection efficiency, fast integration time, and low fake hit rate for farther study. Detectors satisfied with these various performances are required. Specification of pixel sensor performance requirements for MFT sensors are summarized in Table2. In order to fulfill these requirements, Monolithic Active Pixel Sensor(MAPS) based on CMOS technology was adopted as a new pixel sensor for the MFT.

Table 2: Specifications for the MFT sensors[5]

Parameter	Value
Spatial resolution	5 µm
Pixel pitch	25 µm
Detection efficiency	$> 99.5\,\%$
Fake hit rate	$<10^{-5}\mathrm{event}^{-1}\mathrm{pixel}^{-1}$
Integration time	$< 20\,\mu\mathrm{s}$
Sensor thickness	50 µm
Power density	$< 300\,\mathrm{mW/cm^2}$
TID Radiation hardness[a]	2700 krad
NIEL Radiation hardness[b]	$1.7\times10^{13}\,\mathrm{Mev\,n_{eq}/cm^2}$

[a] Total Ionizing Dose. Including a safety factor of ten.
[b] Non Ionizing Energy Loss. Including a safety factor of ten.

3.2 MAPS technology

MAPS for the MFT and the upgraded ITS will be fabricated using the 180 nm CMOS imaging sensor process by TowerJazz[7] as shown in Fig.8. A epitaxial layer, a deep pwell, a PMOS transistor, a NMOS transistor and a nwell diode are laminated on a substrate p^{++}. The process of MAPS allows up to six metal layers and the ability to mount a high-density, low-power circuity on the pixel. Furthermore, the transistor gate oxide thickness of about 3 nm can expect a more resistant TID. The bottom layer is low resistivity($\sim 10\,\Omega$cm) p-type silicon wafer. The epitaxial layer is high resistivity(>1 kΩcm) and acts as the sensitive layer. The generated charges reach a nwell diode which is a collection electrode due to the difference of the applied potential. The deep pwell takes the role as a shield of the nwell of the PMOS transistor. If the deep pwell dose not exist as a layer, the sensor cannot collect the ionized charges entirely at the epitaxial layer because not only a nwell diode but also a nwell which is a bulk of the PMOS transistor absorbs charges.

3.3 ALPIDE design

A discriminator can be installed in each cell by high MAPS technology. So a digital signal converted from an analog signal within the pixel directly reaches the encoding

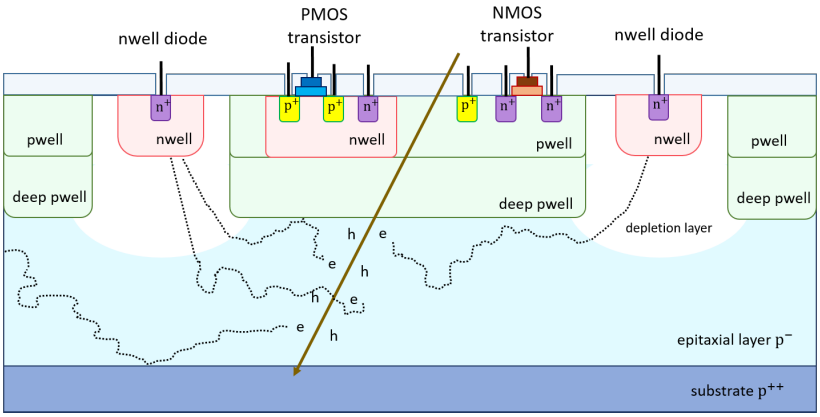

Figure 8: A schematic cross section of a pixel sensor with MAPS technology

circuit which generates the information of the hit point as output data as shown in Fig.9. This makes it possible to improve readout speed and reduce power consumption. The pixel sensor design with these technologies is called an ALPIDE(ALICE pixel detector) design. It is also important to be able to apply reverse substrate bias to the collection diode to manipulate the depletion layer for ALPIDE. An electric field is generated when a reverse bias is applied to a depletion layer formed between the pn junction diode and then diffused charges drift to the collection electrode as shown in Fig.8.

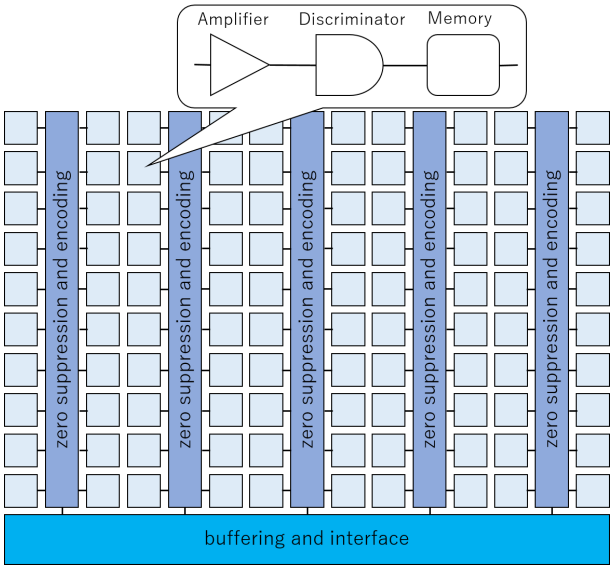

Figure 9: A pixel chip architecture of ALPIDE

3.4 Matrix isolation of ALPIDE chip

SUB (substrate) is biased through the PWELL ring surrounding the peripheral circuit and the NWELL ring as shown in Fig10. The NWELL ring provides isolation of the matrix from the edge of the ALPIDE chip. The PWELL and the deep PWELL

are biased using PWELL contact. SUB and the PWELL are connected through the epitaxial layer if it is not a filled depletion region. The peripheral circuit is mounted in the NWELL and the deep NWELL. This also isolated from the substrate.

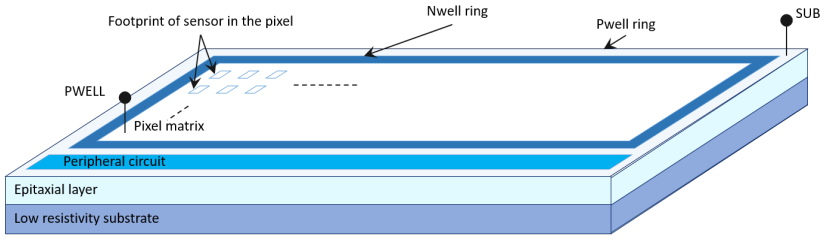

Figure 10: A schematic of matrix isolation in the ALPIDE design.

3.5 Charge generation in the epitaxial layer

The principle of the silicon detectors is based on the energy loss of particles crossing sensory material. As some of the energy is lost it changes the electron-hole pairs. It is then sucked as a current to near collection electrodes. This energy loss of particles is due to the ionization in the substance and the scattering process with electrons in the material. This process is described by the Bethe-Bloch formula

$$-\frac{1}{\rho} < \frac{dE}{dx} >= 4\pi N_A r_e^2 m_e c^2 z^2 \frac{Z}{A}\frac{1}{\beta^2}(\frac{1}{2}\ln(\frac{2\mathrm{m_e c^2}\beta^2\gamma^2\mathrm{T_{max}}}{\mathrm{I^2}}) - \beta^2) \tag{1}$$

$$T_{max} = \frac{2m_e c^2\beta^2\gamma^2}{1 + 2\gamma m_e/M + (m_e/M)^2} \tag{2}$$

$$\gamma = \frac{1}{\sqrt{1-\beta^2}} \tag{3}$$

where N_A is the Avogadro's number, r_e is the classical electron radius, $m_e c^2$ is the rest energy of the electron, z is the charge of the traversing particle in terms of unit charge, Z is the atomic number of the absorption medium(14 for silicon), A is the atomic mass of the absorption medium(28 g/mol for silicon), β is the velocity of the traversing particle in units of c, γ is the Lorentz factor, I is the mean excitation energy(137 eV for silicon) and T_{max} is the maximum energy loss for a particle with mass M in a single silicon. Eq.1 describes only the mean energy loss but not its fluctuations. These fluctuations around the mean value are well described in a Landau distribution[8] for an absorber which is about 300 µm silicone. For thinner absorbers that have approximately 20 µm, fluctuations increase and energy loss is better described by the Bichsel model[9].

3.6 Reverse substrate bias and depletion region

The movement of ionized charges changes with the potential difference between pwell and substrate. Bias is applied to each part as shown in Fig.10 and Fig.11. Then a potential difference is generated due to the difference of resistance values. In a ALPIDE design, The reverse bias voltage $\mathrm{V_{RB}}$ is the bias applied to collection electrode determined by the pixel reset voltage $\mathrm{V_{RST}}$. This then determines the

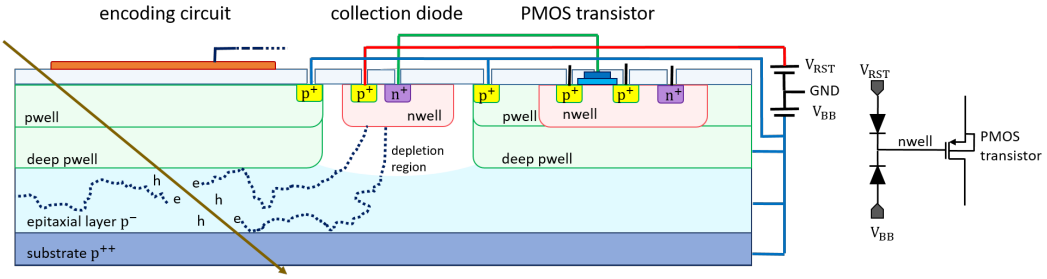

Figure 11: Schematics cross section of ALPIDE design

performance of the NMOS transistor and the reverse substrate bias voltage V_{BB} with $V_{RB} \approx V_{RST} + V_{BB}$. A depletion region where the electric field is generated to the collection electrode direction dependent on V_{BB} is generated between pwell and substrate. This affects the threshold value which is one of the important parameters for characterization. In a case of low V_{BB} as shown in Fig.12 above, since the depletion region is small, there is almost no potential difference required to collect electric charges. The epitaxial layer is filled with the depletion region and a pwell has the lower potential than that of the substrate when higher V_{BB} is applied. Hence, charges can easily flow to the nearby collection electrodes as shown in Fig.12 below. However, it is impossible to apply much high V_{BB} because it can cause a serious breakdown within the structure. In this prototype of ALPIDE, the voltage is operated within -8 V.

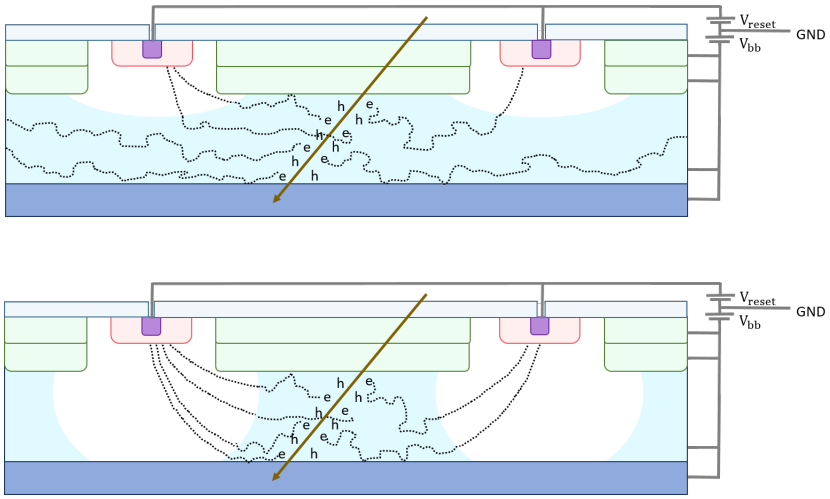

Figure 12: The depletion region of ALPIDE with low (top) and high (bottom) reverse substrate bias.

3.7 Roadmap of ALPIDE development

So far prototypes have been developed and tested in order to install to the MFT and the upgraded ITS. The time line of development and the main features of the prototype are shown in the Fig.13. The final ALPIDE design has already been decided from prototypes by the ITS group.

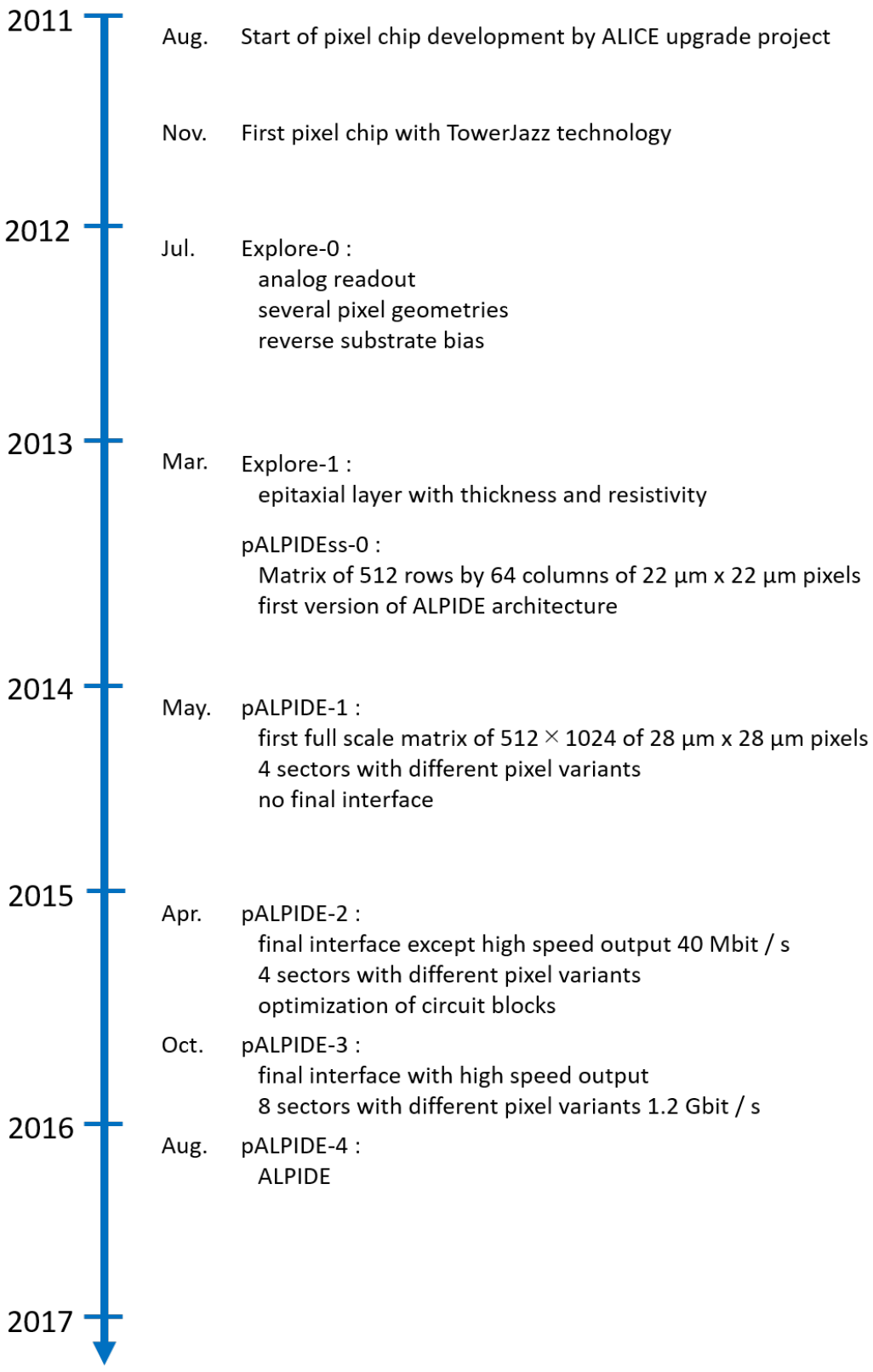

Figure 13: The roadmap of ALPIDE development and features.

4 ALPIDE and pALPIDE structure

In this section, the flow of incident particles that are detected as signals and the ALPIDE and pALPIDE structure are described.

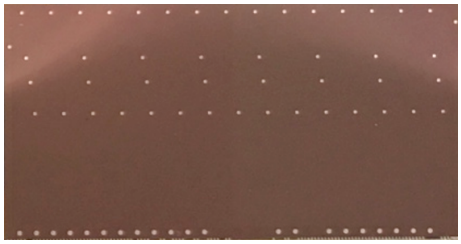

Figure 14: The real pALPIDE-2 chip.

4.1 ALPIDE and pALPIDE rough structure

The very small pixel of approximately 20 µm square consisting ALPIDE or pALPIDE as shown in Fig.15 is made up of the collection electrode, the wave shaping, the amplifier, the discriminator, the state register and the AERD (Address Encoder Reset Decoder). ALPIDE and pALPIDE are an aggregate of 512 × 1024 pixels and are 15.3 mm × 30 mm in size. The flying particles ionize and charges are created and sucked into the collection electrodes to form a signal as mentioned above. The potential drops in about 100 ns from a base line and the potential return to its original position in about 100 µs by the reset voltage as shown in bottom left of Fig16. Next, at the front end part, the signal is amplified and converted from the analog signal to digital signal as shown in lower middle section of Fig.16. Then, it is discriminated by the external signal STROBE which is the trigger in state register as shown in bottom right of Fig16. There are two modes in the strobe, one is determined by the pulse width of the above trigger. Another is always active except during the AERD read out. Finally, the AERD sends the hit point and timing to chip periphery.

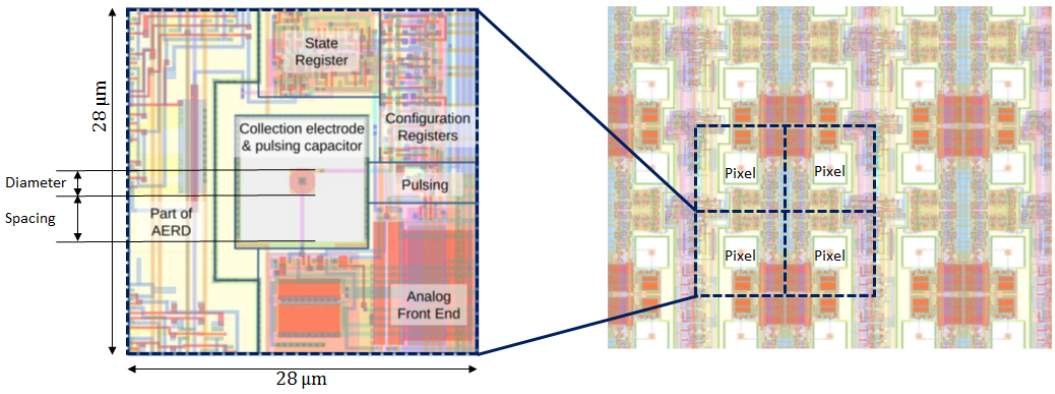

Figure 15: The pixel layout and pixel matrix details of a pALPIDE-2[10].

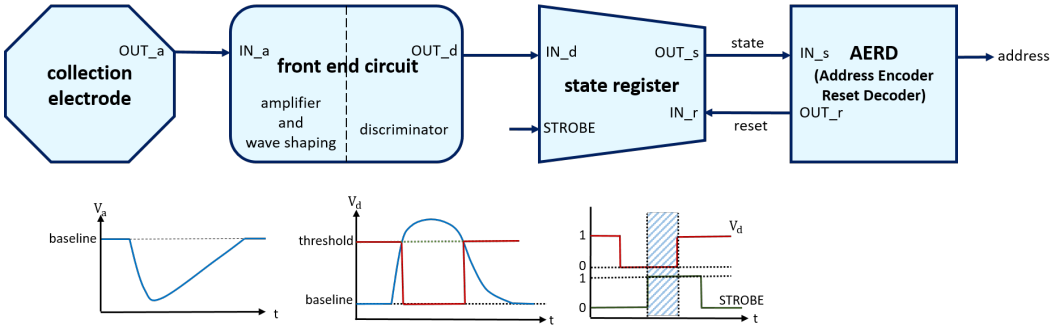

Figure 16: The schematic of a pixel circuit of pALPIDE and its signal flow.

4.2 Detail of the front end circuit of pALPIDE

A pALPIDE is divided into 4 sectors (512 × 256 pixels) for versio 2 and 8 sectors (512 × 128 pixels) for version 3, and different front end circuits are mounted respectively. The details of the front end circuit of version 2 and 3 of pALPIDE used in this thesis are described below.

4.2.1 pALPIDE-2

The pixel standard of pALPIDE-1 and pALPIDE-2 are 28 µm×28 µm and the pALPIDE-2 front end circuits are similar to version 1.

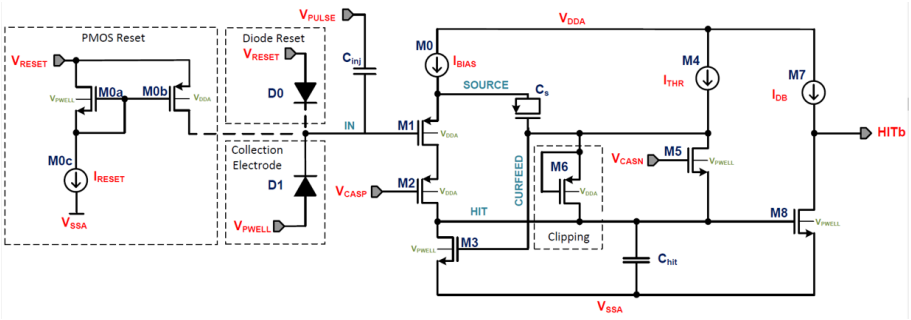

Figure 17: A front end circuit diagram of a pALPIDE-2 including all possible variations[11].

Table 3: Details of the front end circuit of pALPIDE-2

Sector	Diameter [µm]	Spacing [µm]	Reset	Input transistor width [µm]
0	2	2	PMOS	0.22
1	2	2	PMOS	0.92
2	2	4	PMOS	0.22
3	2	4	Diode	0.22

The reset current depends on the sensor leakage and the signal amplitude for the diode reset mechanism as shown in Fig.18 left. It is limited by adjusting the current

I_{RESET} for PMOS reset mechanism as shown in Fig.18 right. The charge can be injected by applying voltage V_{PULSE} to the capacitor C_{inj} when testing the property evaluation. By manipulating the volume of the current I_{THR} flowing to the input PMOS transistor M1 and the current I_{BIAS} flowing to the NMOS transistor M5, it is possible to change the amplification and shaping factor of the signal affecting its threshold and noise. The NMOS transister M5 in the circuit can also adjust the V_{CASN} which affects the threshold and noise. The variation of V_{CASN} allows the base line change of the signal flowing to the gate of the NMOS transistor M8. The transistor M6 limits the pulse which reaches M8 when V_{HIT} exceeds $V_{COURFEED}$. The current source M7 and the transistor M8 are present to discriminate and invert the signal. All of these parameters can not be adjusted for each pixel, and they are applied to the whole chip. The diameter is equal to the collection electrode diameter and the spacing is the distance between NWELL and PWELL. The input transistor indicates the size of the PMOS transistor M1 in the circuit.

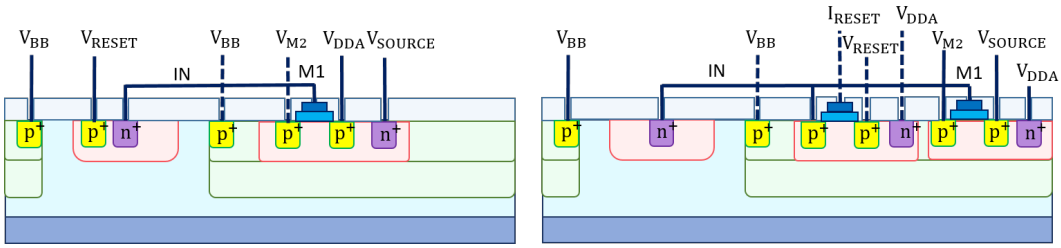

Figure 18: A schematic of the diode reset (left) and PMOS reset (right).

4.2.2 pALPIDE-3

Since the number of transistors for a good shaping pulse is added, the pixel standard is larger than version 2 and it is 29.24 µm×26.88 µm (W×H).

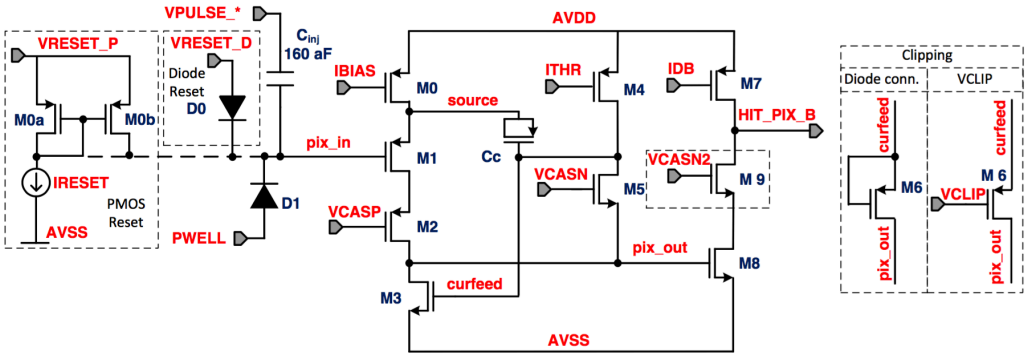

Figure 19: The front end circuit of pALPIDE-3 including all possible variations[11].

The spacing between NWELL and PWELL in the collection diode affects the change of the pixel input with the reverse bias voltage. The size is 2 µm for all sectors except sector 5. The body terminal of the transistor which affects the threshold is connected to V_{DDA} or V_{SOURCE} as shown in Fig.20. The PMOS transistor M6 allows to get a more uniform pulse duration for sector 3,4,5 and 7 with V_{clip}. Without this clipping,

Table 4: Details of the front end circuit of pALPIDE-3.

Sector	size (M3, M5, M6, M8)	V_{CASN2}	Clipping	M1 bulk	Reset	Spacing
0	optimized size	yes	diode conn.	AVDD	Diode	2 µm
1	optimized size	no	diode conn.	AVDD	Diode	2 µm
2	as in pALPIDE-1,2	no	diode conn.	AVDD	Diode	2 µm
3	optimized size	yes	V_{clip}	AVDD	Diode	2 µm
4	optimized size	yes	V_{clip}	Source	Diode	2 µm
5	optimized size	yes	V_{clip}	Source	Diode	3 µm
6	as in pALPIDE-1,2	no	diode conn.	AVDD	PMOS	2 µm
7	optimized size	yes	V_{clip}	AVDD	PMOS	2 µm

the high current would flow into the circuit and the pulse would quickly rise. Then it would takes a long time to return to baseline. A NMOS transistor is added between M7 and M8 but there is no significant impact on the characterization in these tests. In addition, the size of the transistor M3, M5, M6 and M8 was optimized via simulation study.

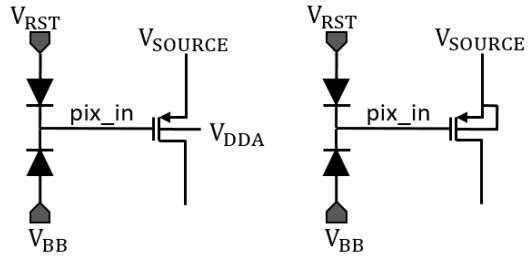

Figure 20: The schematic of the input transistor M1. Connect V_{DDA} (right) or connect V_{SOURCE} (left) to the body terminal.

4.2.3 Front end biasing parameters

The ALPIDE and pALPIDE have eleven 8 bit DACs (Digital Analog Converter), 6 voltage and 5 current DACs on the chip periphery. The current voltage in the front end circuit can be controlled by manipulating the value of the DAC shown in Tab.5 and Tab.6 from the outside raging from 0 to 255.

4.3 Digital part of pALPIDE

The digital part of the pALPIDE containing three registers : a state register, a mask register, and a pulse register as shown Fig.21. When there is a part where the signal PIX_OUT_B comes from the front end circuit and the STROBE signal STROBE_B sent from the chip peripheral overlap, The hit information is created in the state register and then out put to AERD. The state is reset by the reset signal PRST or PIXRST generated by AERD. When a mask register is activated, it prevents the information in the state register from being sent to AERD. This allows for restriction readings of hot pixels that cause malfunction or intense noise.

Table 5: Overview of the biasing parameters

Bias	Minimum	Maximum	Nominal setting	Nominal value
I_{BIAS}	0 nA	80 nA	64	20 nA
I_{THR}	0 nA	80 nA	51	0.5 nA
I_{DB}	0 nA	80 nA	64	10 nA
I_{RESET}	0.7 nA	26 pA	50	5 pA
I_{AUX}	-	-	-	-
V_{CASP}	0 V	1.8 V	86	0.6 V
V_{CASN}	0 V	1.8 V	57	0.4 V
V_{CASN2}	0 V	1.8 V	62	0.44 V
V_{CLIP}	0 V	1.8 V	0	0 V
V_{RESET_P}	0.37 V	1.8 V	117	1.2 V
V_{RESET_D}	0.37 V	1.8 V	147	1.4 V
V_{PULSE_LOW}	0.37 V	1.8 V	0	0.37 V
V_{PULSE_HIGH}	0.37 V	1.8 V	255	1.8 V

Table 6: Scaling factors of current DAC

DAC	Scaling from DAC to matrix
I_{BIAS}	1:128
I_{THR}	1:4096
I_{DB}	1:256
I_{RESET}	$\approx 1 : 4 \times 10^5$

The function of the front end or state register can be tested by activating the pulse register. The charge reaches C_{inj} in Fig.17 and Fig.19 when this is operated.

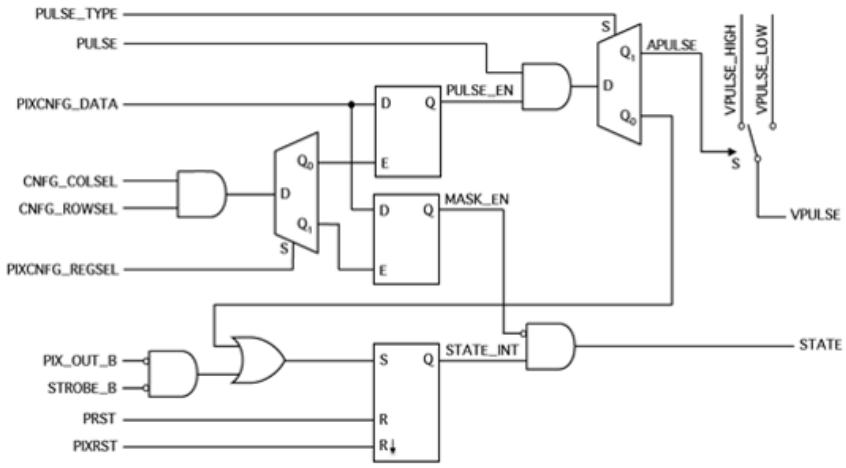

Figure 21: A schematic of a section of the state register in a pALPIDE[12].

4.4 Front end circuit of ALPIDE

The final ALPIDE design is decided from prototypes by the ITS group which started the study earlier than the MFT group, but ALPIDE and pALPIDE still need to be tested to optimize the settings and it is necessary to accumulate the experience in order to operate ALPIDE for the MFT institutes. The last design of the circuit is shown in Fig.22 and the parameters that are used for sector 5 of pALPIDE-3 : diode reset, optimized size for M3, M5, M6 and M8, M1 bulk connected to source, input transistor M1 size of 0.92 µm×0.18 µm, clipping point by V_{CLIP}, including V_{CASN2} and spacing of 3 µm.

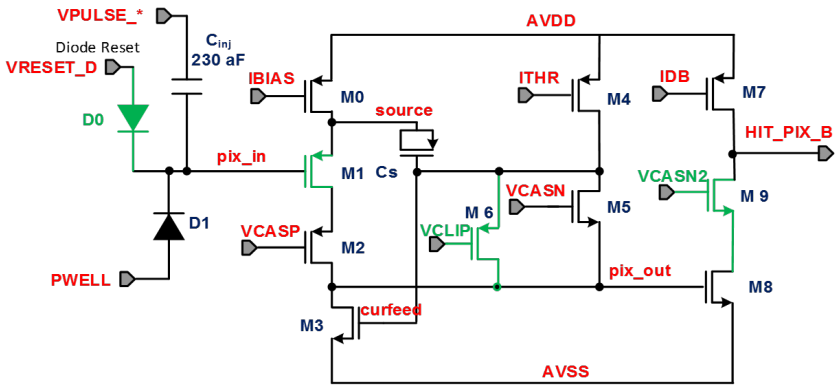

Figure 22: A schematic of the front end circuit in pALPIDE[11].

5 pALPIDE version 2 and 3 characterization

Results of the characterization of the pALPIDE-2 and the pALPIDE-3 are described in this section.

5.1 Construction of the experimental environment for pALPIDE

In the pALPIDE characterization, we used a board, called a carrier board shown in Fig.23 left, loaded with the chip, a DAQ (Data Acquisition) board shown in Fig.23 right to read and write data and control the current voltage value on the front end circuit. A power supply is used to apply the current to the circuit of the chip and a computer for accumulating the data and giving orders to the DAQ board. The DAQ board with the FPGA (Field Programmable Gate Array) manufactured by ALTERA company is used in this characterization. The carry board and the DAQ board are directly connected, and the DAQ board and the PC are connected by a USB cable. The current and the voltage are supplied from a power supply as shown in Fig24. Fig25 shows the first experimental system built in Japan by me. In order to start the experiment, since a lot of noise is detected, the carrier board and the DAQ board must be characterized in the black box.

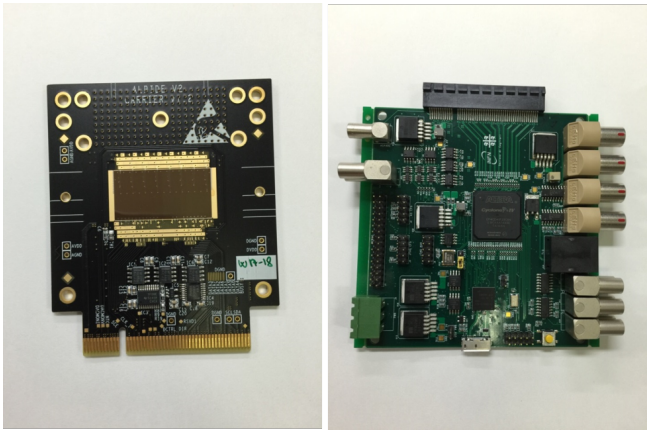

Figure 23: The carrier board (left) and DAQ board (right).

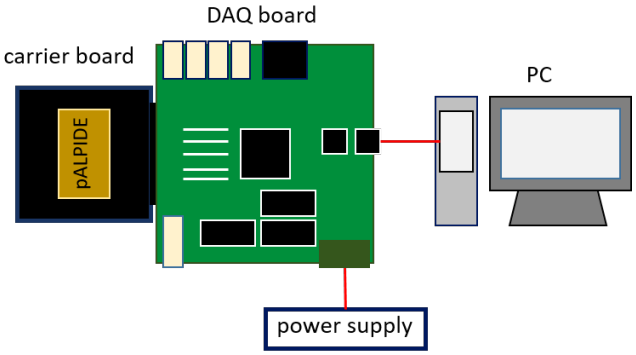

Figure 24: The wiring diagram of the equipment.

Figure 25: The test environment at Hiroshima University.

5.2 Threshold scan

The threshold value is one of the most important parameters for the sensor design. The low threshold value allows a high detection efficiency, but the fake hit rate is also higher at the same time. The value of the threshold is calculated with the following function using charges q_{inj} which then are injected to C_{inj} on the front end circuit and then charges q_{thr} when the pixel recognizes the hit.

$$f(q_{inj}) = \frac{1}{2}N_{inj}(1 + \mathrm{erf}(\frac{q_{inj} - q_{thr}}{\sqrt{2}\sigma}) \tag{4}$$

However N_{inj} equals the number of trials to pass one charge to the circuit but in this characterization set to 50. q_{thr} is treated as the threshold value and σ is used as the noise. The relationship between number of trials, the injected charges, the threshold, and the noise values at that pixel are shown in the Fig.26. The intermediate charge from the beginning of rise to the end is a threshold value and its fluctuation is thee noise value. In other words, the threshold is a value indicating the easiness of a hit detection. If the threshold value is small, it is possible to recognize a smaller signal which has not been recognized so far as a hit.

5.3 Threshold and noise

In order to optimize the front end circuit on a pixel, we need to know how the threshold depends on the settings such as back bias, I_{THR}, V_{CASN}, etc. In this study, only the I_{THR} was changed, and the behavior of the threshold was examined. Fig.27 shows the threshold value distribution in each sector for pALPIDE-2. Values were measured with three I_{THR} values of 10, 50 and 100 respectively. The peaks of the distribution became gentler as the current value increased. Fig.28 shows the results of measurements with $V_{BB} = -3\,V$ and -6V, and the changing V_{RST} for the applied back bias for pALPIDE-2. Since only a large change is seen in sector 3, diode reset is greatly affected by back bias and V_{RST}. Fig.29 and Fig.30 are plots

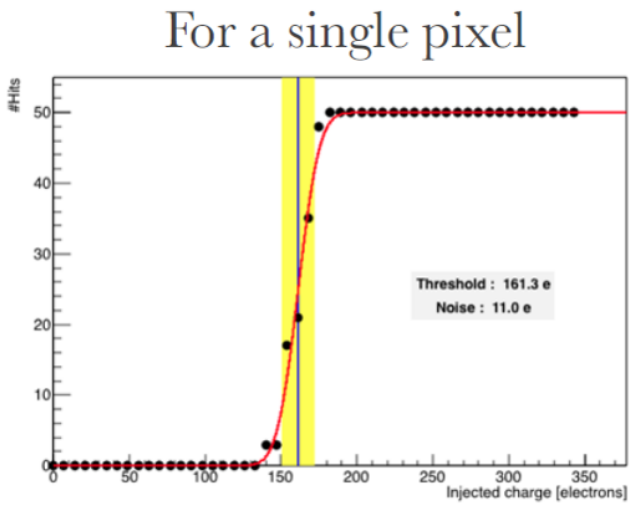

Figure 26: The number of hit charges as the function of the injected charges.

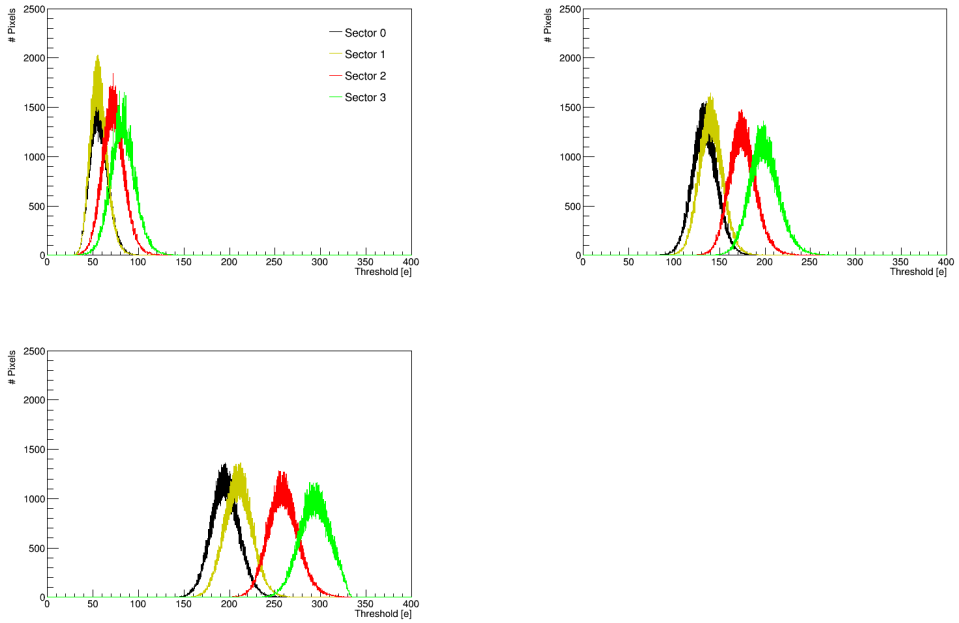

Figure 27: Threshold values and their numbers in each sector for pALPIDE-2 with $I_{THR} = 10$ (upper left), $I_{THR} = 50$ (upper right) and $I_{THR} = 100$ (bottom left).

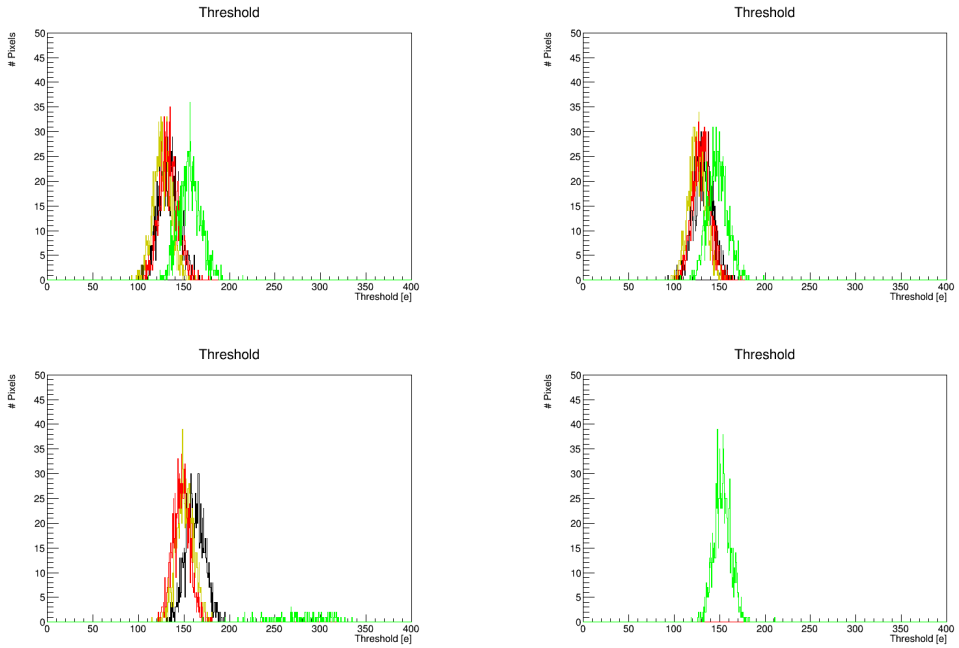

Figure 28: Threshold values and their numbers in each sector for pALPIDE-2 with $I_{THR} = 50$ / $V_{BB} = -3\,V$ / $V_{RST} = 117$ (upper left) and $V_{RST} = 140$ (upper right), and $I_{THR} = 50$ / $V_{BB} = -6\,V$ / $V_{RST} = 117$ (bottom left) and $V_{RST} = 180$ (bottom right).

of I_{THR} as a function of threshold and noise values for pALPIDE-2 with changing back bias. From both results it turned out that VBB contributed significantly to sector 3. Next, the threshold value of pALPIDE-3 was measured. Fig.31 shows the results of the threshold and noise measured in the same way as in Fig.28. Since the thresholds of sectors 4 and 5 are lower, we can see that the bulk of M1 on the front end relates to the contribution to the circuit of the source connection. It also turns out that the noise increases with a diode reset. Fig.32 and Fig.33 are plots of I_{THR} as a function of the threshold and noise values for pALPIDE-3 with changing back bias. In sector 5, as the back bias decreases, the threshold changes in the decreasing direction, and the noise also decreases.

5.4 Fake hit rate

The fake hit rate is a value indicating the rate at which pixel erroneously recognizes hit. The fake hit has some causes such as pixel breakdown, and it is very important to study this ratio because it must be eliminated for measurement. The rate is calculated by Eq.5.

$$\text{Fake hit rate} = \frac{\text{hit}}{\text{event} \times \text{pixels/sector}} \tag{5}$$

where hit is number of recognized hit. Event is number of trial of measurements. Pixels are the numbers in 1024×512 pixels and sector is 8 for pALPIDE-3. I_{THR} or V_{CASN} dependence of the rate in each sector for pALPIDE-3 are shown in Fig34 and Fig35. MFT will require a fake hit rate $< 10^{-5}$. The rate increases as V_{BB} decreases for vs I_{THR}, and for vs V_{CASN} the rate decreases as I_{THR} increases. In

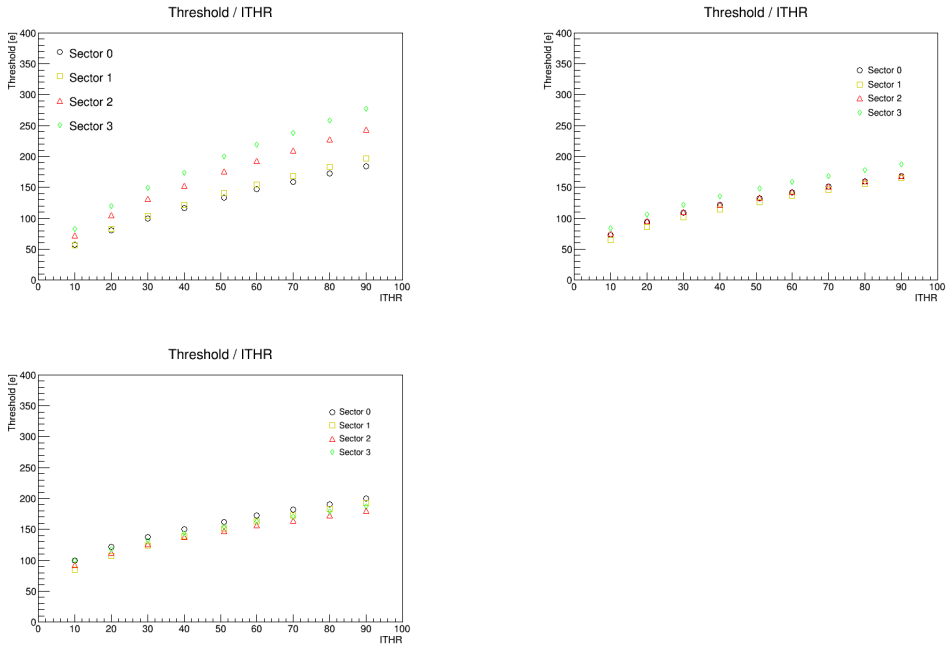

Figure 29: Threshold values vs I_{THR} in each sector for pALPIDE-2 with $V_{BB} = -0\,V$ (upper left) ,-3 V (upper right) and -6 V (bottom left).

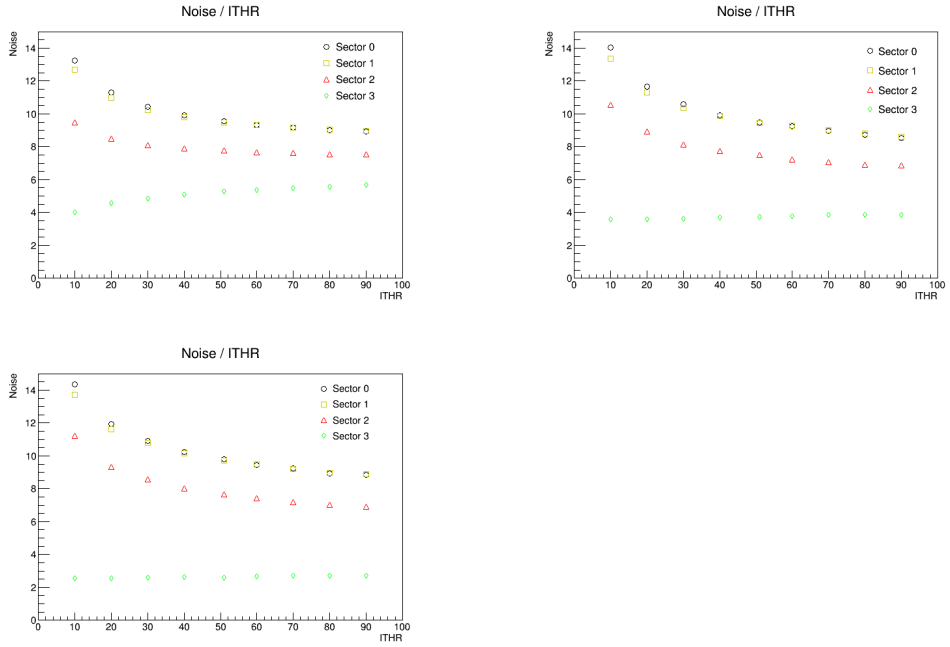

Figure 30: Noise values vs I_{THR} in each sector for pALPIDE-2 with $V_{BB} = -0\,V$ (upper left) ,-3 V (upper right) and -6 V (bottom left).

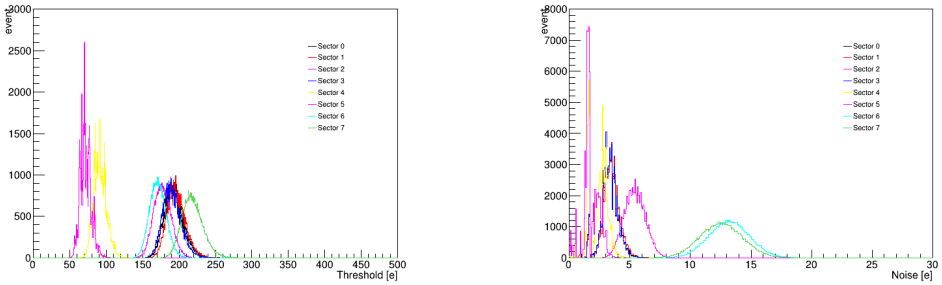

Figure 31: Threshold (left) and noise (right) values and their number in each sector for pALPIDE-3 with $V_{BB} = -0\,V$ / $I_{THR} = 50$.

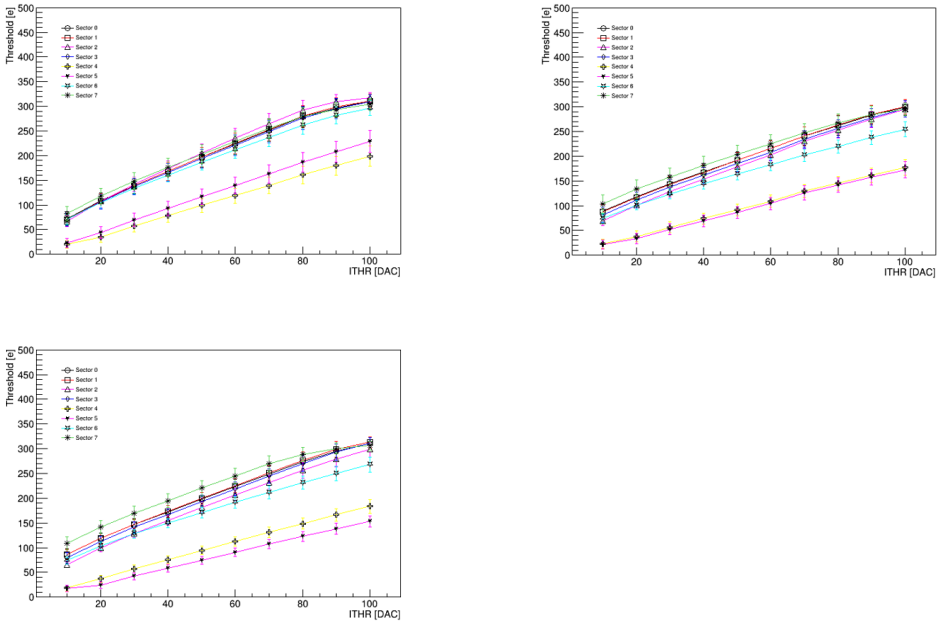

Figure 32: The threshold values vs I_{THR} in each sector for pALPIDE-3 with $V_{BB} = -0\,V$ (upper left) ,-3 V (upper right) and -6 V (bottom left).

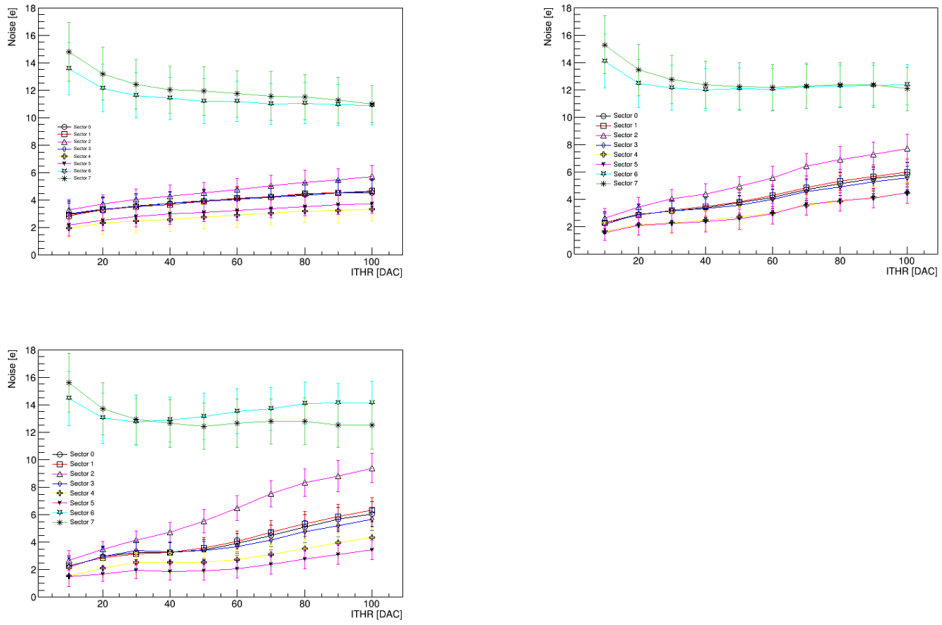

Figure 33: The noise values vs I_{THR} in each sector for pALPIDE-3 with $V_{BB} = -0\,V$ (upper left) ,-3 V (upper right) and -6 V (bottom left).

addition, it is a volume of 10^{-5} or less except for sector 6 in the V_{CASN} dependence.

5.5 Temperature dependence

The carrier board has a function to measure the temperature of the whole chip. The relationship between temperature change and the noise from the start of the measurement was investigated. The time dependence of temperature is shown in the left Fig.36, and the time dependence of the noise is shown in the right figure. The temperature rises with the passage of time, reaching equilibrium in about 7 hours. The noise also rises as the temperature rises. However, even when the temperature reaches equilibrium, the noise fluctuates in a range of several percentage points.

5.6 Source measurement

The radioactive source of 1 MBq shown in Fig.37 was used and, it is separated by more than 5mm from pALPIDE so that the particles spread throughout the plate. The plot of the hit map when the source is placed and it is not placed is shown in Fig.38. It is obvious that a large amount of radiation was detected on the side using a radiation source. Since it was confirmed that radiation could be detected, I clustered simultaneously detected particles together to know where the incident took place. A hit pixel adjoins neighboring hit pixels as a cluster and repeats in the same event as shown in Fig39. Fig40 is a hit map and a plot that shows a cluster in it. However, since the difference in the number of ionized charges can not be identified, the center of the cluster is the injected point. The number of pixels included in the cluster is called the cluster size and its distribution is shown in left of Fig41. It can be seen that there is a large amount of one pixel which

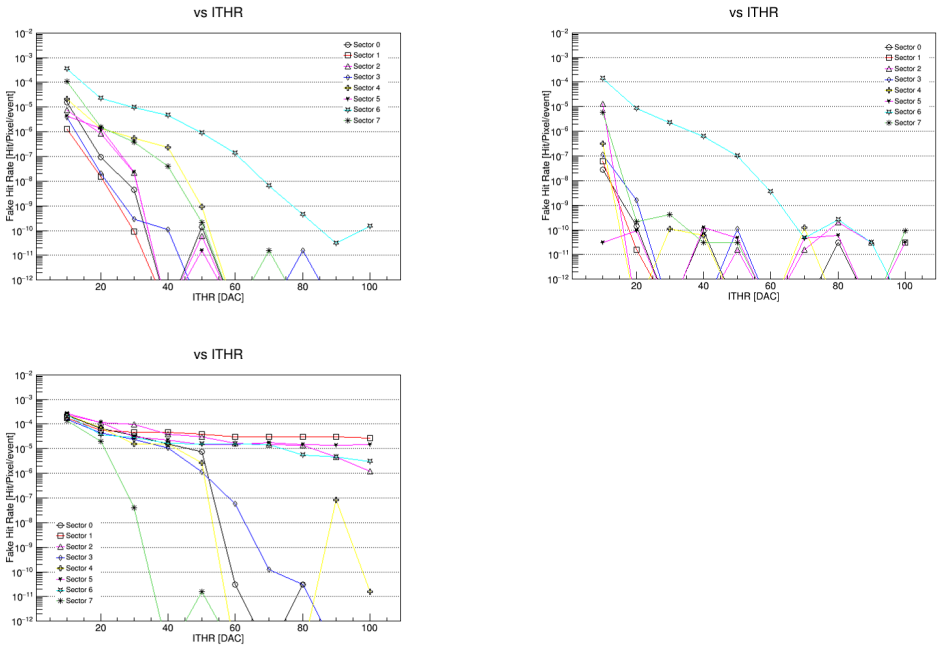

Figure 34: I_{THR} dependence of fake hit rate in each sector for pALPIDE-3 with $V_{BB} = -0\,V$ (upper left) ,-3 V (upper right) and -6 V (bottom left).

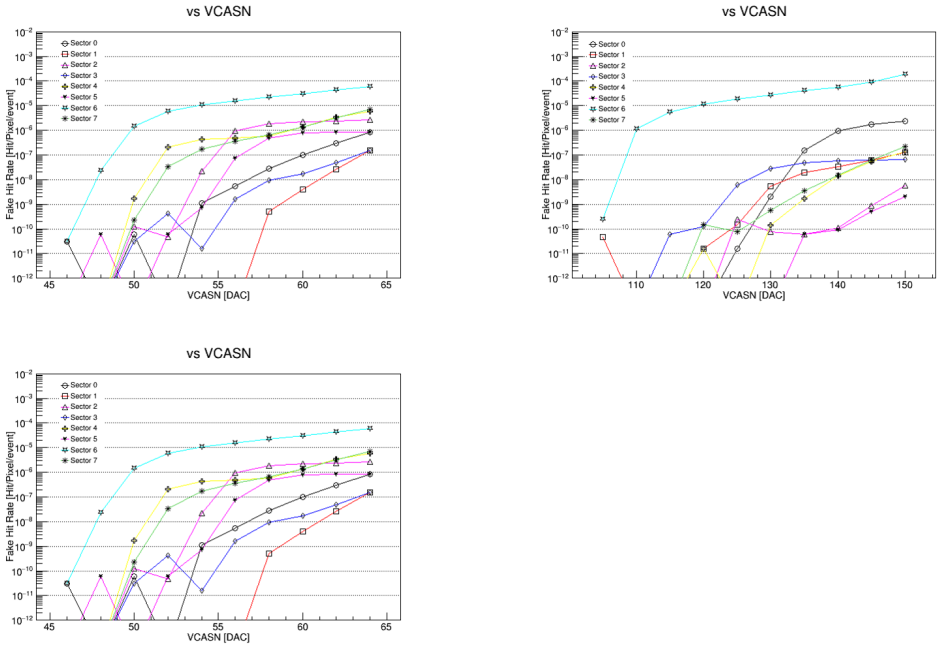

Figure 35: V_{CASN} dependence of fake hit rate in each sector for pALPIDE-3 with $V_{BB} = -0\,V$ (upper left) ,-3 V (upper right) and -6 V (bottom left).

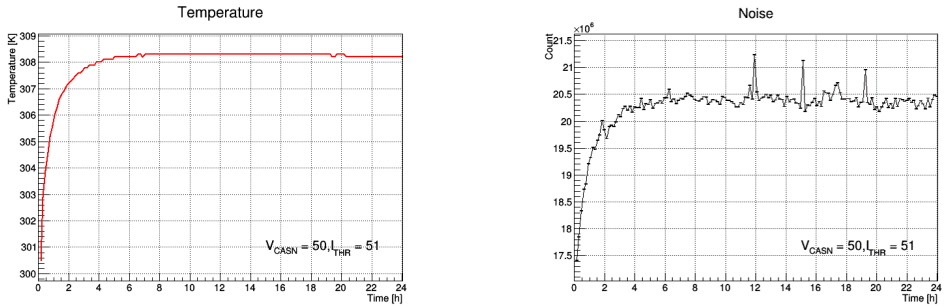

Figure 36: Temperature of pALPIDE over time and number of hits without a source at that time.

Figure 37: Source (Fe55) used in the experiment.

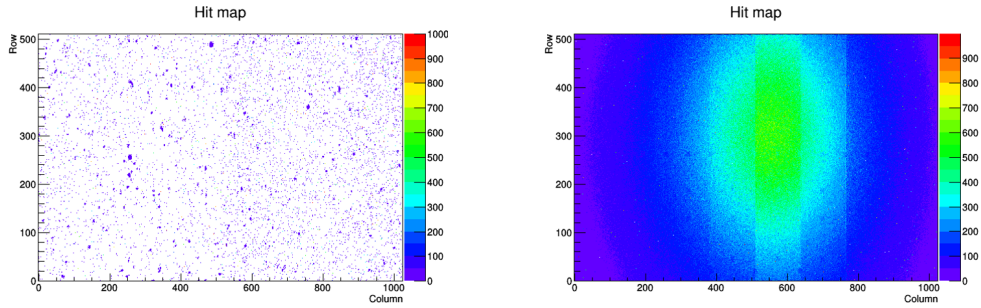

Figure 38: Hit map without source (left) and with source (right) for pALPIDE-3.

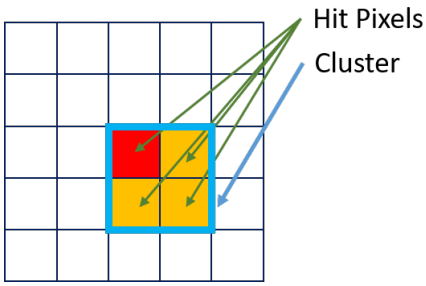

Figure 39: Clustering method.

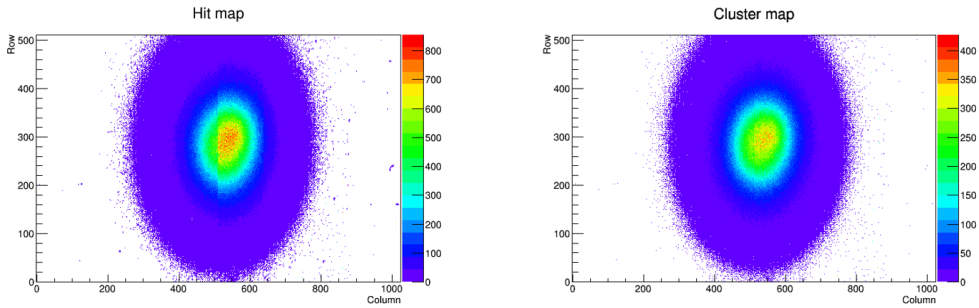

Figure 40: Hit map (left) and cluster (right) map for pALPIDE-3 with source.

is recognized as a pixel causing malfunction in the left plot. Therefore, the value obtained by subtracting the distribution with source (blue line) from the distribution without source (red line) can be a correct cluster size distribution shown in right of Fig41. The I_{THR} dependence of cluster size distribution differentiated in each sector is shown in Fig.42. The maximum size was at around $I_{THR} = 50$, and it had approximately 2 pixels in each cluster.

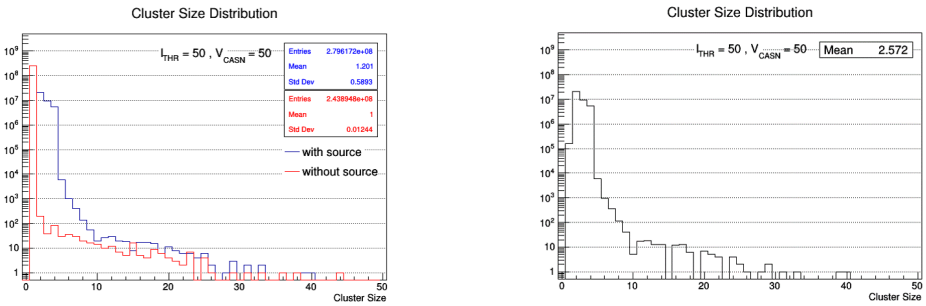

Figure 41: Cluster size distribution for pALPIDE-3 with source (left, red line) and without source (left, blue line), and its difference (right).

5.7 Relative efficiency

Efficiency is generally an indicator showing how accurately the incident particle is detected, but the relative efficiency mentioned here is the ratio of the efficiency based on the lowest I_{THR} value. Both the relative efficiency and the fake hit rate

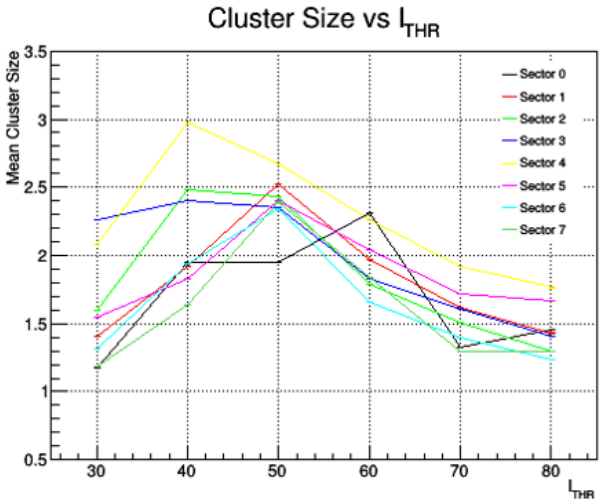

Figure 42: I_{THR} dependence of cluster size.

are decreasing with increasing I_{THR} as shown in Fig.43.

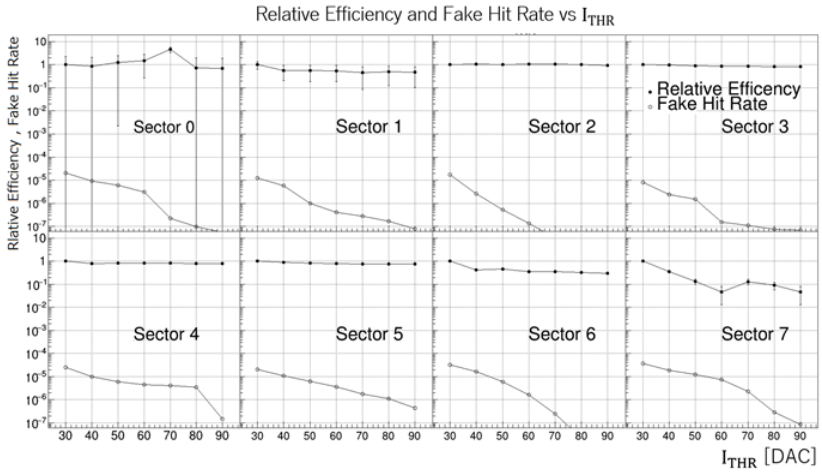

Figure 43: I_{THR} dependence of relative efficiency and the fake hit rate.

6 Summary and Outlook

pALPIDE version 2 and 3 are characterized in this thesis. The pALPIDE characterization is the first attempt in Japan. I checked the ALPIDE design performance because we use the ALPIDE design decided by the ITS group which started the study earlier than the MFT group. pALPIDE had a small percentage of uncertainty for each measurement even at a constant temperature. The relative efficiency and fake hit rate decreased due to the decrease of the threshold with the rise of I_{THR}. These results obtained by the characterization are very important data for us to operate MFT. In the future, we will characterize the multiple ALPIDE such as ladder and disk at the same time and aim for implementation in 2019.

Acknowledgment

First of all I would like to thank my parents. Thank you for letting me go to college without inconvenience. I was able to successfully complete master's course. Next, I would like to express my thanks to Prof. K.Shigaki who instructed me directly from the university 4th year. Thank you so much for giving me the theme of this thesis and various advices. I think that it was impossible to complete the thesis without his support. I also appreciate the all stuff in quark laboratory. Thank you for giving me kind but very tough advice. I was able to deepen my understanding of my study and train mental strength. And I would like to thank senior in Hiroshima University. Thank you for telling me what I do not understand. It helped to complete this work. Finally I thank Mr. Yamakawa of the same grade, thank you for everything. In addition, I would like to express my thank to ALICE collaboration.

Reference

[1] LHC ALICE -ALICE JAPAN- URL:http://alice-j.org/

[2] ALICE Collaboration, J.Adam et al., Technical Design Report for the Upgrade of the ALICE Inner Tracking System, CERN-LHCC-2013-024 (2014).

[3] ALICE Collaboration, J.Adam et al., Addendum to the Technical Design Report for the Upgrade of the ALICE Time Projection Chamber, CERN-LHCC-2015-002 (2015).

[4] ALICE Collaboration, J.Adam et al., Upgrade of the ALICE Readout & Trigger System, CERN-LHC-2013-019 (2013).

[5] ALICE Collaboration, J.Adam et al., Technical Design Report for the Muon Forward Tracker, CERN-LHCC-2015-001 (2015).

[6] ALICE Collaboration, J.Adam et al., Technical Design Report for the Upgrade of the Online-Offline Computing System,CERN-LHCC-2015-006 (2015).

[7] TowerJazz, URL:http://www.jazzsemi.com/

[8] L.Landau, On the energy loss of fast particles by ionization, J. Phys. (USSR) 8 (1944).

[9] H.Bichsel, Straggling in thin silicon detectors, Rev. Mod. Phys. 60 (1988).

[10] ALICE Collaboration, T.Kugathasan, ALPIDE-Pixel Design, ITS Pixel Chip Review (2013).

[11] ALICE Collaboration, C.Gao (CCNU), ALPIDE Front End Circuit, 7th ALICE ITS Upgrade, MFT, and O2 Asian Workshop (2016).

[12] ALICE Collaboration, M.Krammer et al., Study and Development of a novel Silicon Pixel Detector for the Upgrade of the ALICE Inner Tracking System, CERN-THESIS-2015-255 (2015).

[13] ALICE Collaboration, R,Felix et al., Studies for the ALICE Inner Tracking System Upgrade, CERN-THESIS-2016-033 (2016).